Supplementary information for

Multivalent binding and DNA length-dependent photo-adduct formation of $Ru(TAP)_3^{2+}$

Willem Vanderlinden,[*a,b] Pauline J. Kolbeck,[a] Wout Frederickx,[b] Sebastian F. Konrad,[a] Thomas Nicolaus,[a] Carola Lampe,[a] Alexander S. Urban,[a] Cécile Moucheron[c] and Jan Lipfert[a]

Contents:

Materials and Methods

DNA substrates. For the magnetic tweezer measurements a 7.9-kbp DNA construct, prepared as described previously [1], was used. In brief, PCR-generated DNA fragments (~600 bp) labeled with multiple biotin or digoxigenin groups were ligated to the DNA, to bind magnetic beads and the flow cell surface, respectively. Linear DNA fragments (486 bp) used for atomic force microscopy imaging were obtained by PCR amplification of a synthetic DNA fragment (gBlock fragment; Integrated DNA Technologies). PCR products were purified from primers, proteins and salts using a PCR Cleanup kit (QIAquick PCR Purification Kit – Qiagen) and resuspended in 10 mM phosphate buffer. To test the effect of DNA length on the spectroscopic properties of $Ru(TAP)_3^{2+}$, we used phage lambda DNA (NEB; N3011L) that was dialyzed overnight against 10 mM phosphate buffer to remove the EDTA used for storage. In addition we tested a 32 bp double stranded fragment that was obtained by annealing the complementary oligodeoxynucleotides 5' ACG TCA GTC AGC ATC AGA GTT TTC CCG TGA AG 3' and 5' CTT CAC GGG AAA ACT CTG ATG CTG ACT GAC GT 3'.

Ruthenium complexes. Racemic $Ru(TAP)_3Cl_2$ was synthesized following published methods [2]. The powder was dissolved in 10 mM phosphate buffer and the concentration was measured using the extenction coefficient ε_{437nm} = 13000 $M^{-1}cm^{-1}$). Racemic $Ru(Phen)_3Cl_2$ was obtained commercially (Sigma-Aldrich; 904767). The powder was dissolved in 10 mM phosphate buffer and the concentration was assessed spectroscopically using the extinction at 445 nm (ε_{445nm} = 19000$M^{-1}cm^{-1}$).

Buffers. All experiments were peformed in 10 mM phosphate buffer, pH = 7.0.

Atomic force microscopy imaging. Samples were prepared by incubating 486 bp linear DNA (1 ng/μL) and $Ru(TAP)_3^{2+}$ at different concentrations in phosphate buffer (pH = 7.0), for 10 min. After incubation, 20 μL of the sample was drop-casted on poly-L-lysine (0.01 % w/v) coated muscovite mica (West Chester, USA). After 30 s, the substrates were gently rinsed using 20 mL of milliQ water and dried using a gentle stream of filtered N_2 gas. Atomic force microscopy imaging was performed on a commercial Multimode AFM, equipped with a Nanoscope III controller and a type E scanner. Images were recorded in amplitude modulation mode under ambient conditions and using silicon cantilevers (Nanoworld; type SSS-NCH; resonance frequency ≈300 kHz; typical end-radius 2 nm). Scans of 1 μm^2 were recorded at 4 Hz line frequency, with optimized feedback parameters and at 512 × 512 pixels. For image processing, Scanning Probe Image Processor (SPIP v6.4; Image Metrology) was employed. Image

processing involved background correction using global fitting with a third-order polynomial, and line-by-line correction through the histogram alignment routine. Data analysis involved tracing of the DNA contours with a step-length l = 5 nm using the algorithm by Wiggins *et al.* [3]

Magnetic tweezers. We used a custom-built MT setup, described previously [4, 5], with a pair of 5 x 5 x 5 mm^3 permanent magnets (W-05-N50-G, Supermagnete, Switzerland) oriented in vertical configuration [6] and with a gap size of 1 mm. A DC-Motor (M-126.PD2, PI, Germany) controlled the distance between the flow cell and magnets, and another DC-Motor (C-150.PD, PI, Germany) was used to rotate the magnets. A 40x oil immersion objective (UPLFLN 40x, Olympus, Japan) was used to image the beads onto a CMOS sensor camera (12M Falcon2, Teledyne Dalsa, Canada) with a field of view of 400 x 300 μm^2. Images were recorded at 58 Hz and transferred to a frame grabber (PCIe 1433, NI, USA). A custom-written tracking software analyzed the images to yield the (x,y,z) coordinates of all beads in real time [7]. A LED (69647, Lumitronix LED Technik GmbH, Germany) was illuminated the sample. For tracking the z-position of the beads, look-up tables (LUT) were generated to relate the defocused pattern of the bead to its height [8]. The LUT was generated by moving the objective using a piezo stage (Pifoc P-726.1CD, PI, Germany). Flow cells were built from two glass coverslips (24 x 60 mm, Carl Roth, Germany). To attach the DNA to the flow cell, the bottom coverslip was first modified with (3-Glycidoxypropyl)trimethoxysilane (abcr GmbH, Germany). Afterwards, 75 µl of a 5000x diluted stock solution of polystyrene beads (Polysciences, USA) in ethanol (Carl Roth, Germany) was dropcasted on the silanized slides, dried in a closed container, and baked at 80°C for 1 min, to serve as reference beads. A laser cutter was used to produce openings with a radius of 1 mm in the top coverslip, to enable liquid exchange. The two coverslips were glued together by a single layer of melted Parafilm (Carl Roth, Germany), comprising a ~ 50 µL channel connecting the inlet and outlet opening of the flow cell. Following flow cell assembly, 100 µg/ml anti-digoxigenin (Roche, Switzerland) in 1x PBS was introduced and incubated for 2 h. To reduce non-specific interactions, the flow cell was flushed with 800 µl of 25 mg/ml bovine serum albumin (Carl Roth, Germany), incubated for 1 h and rinsed with 1 ml of 1x PBS. For all measurements, we used 1.0 µm diameter MyOne magnetic beads (Life Technologies, USA). The DNA construct was attached to streptavidin coated beads by incubating 0.5 µl of picomolar DNA stock solution and 2 µl MyOne beads in 250 µl 1x PBS (Sigma-Aldrich, USA) for 5 min. Subsequently, the bead-coupled DNA solution was introduced in the flow cell for 5 min to allow formation of digoxigenin-anti-digoxigenin bonds. Subsequently, the flow cell was rinsed with 2 ml of 1x PBS to flush out unbound beads. Next, the magnet was mounted, which constrains the rotation and applies an upward force on the beads. After installing the magnets, selected beads were tested for the presence of multiple tethers, and torsional constraint, by measuring their response to forces and torques. The presence of multiple tethers was assessed by rotating the magnet to introduce negative supercoiling under high tension ($F \geq 5$ pN.) In the case of a single DNA tether, high tension impedes the formation of plectonemes at negative linking differences. As a result, no height change is observed. In contrast, in case of multiple tethers are attached to a bead, introduction of negative supercoiling results in braiding, decreasing the z-extension of the bead. Beads bound by multiple tethers are discarded from further analysis. To assess whether DNA tethers were torsionally constrained, positive linking differences are introduced at low force (0.4 pN). In torsionally constrained DNA tethers, this results in plectoneme formation, thereby decreasing the z-extension. In nicked DNA tethers, no linking difference can be introduced and the z-extension remains constant on rotation of the magnet. Following bead selection and testing, the buffer in the flowcell was exchanged for a 10 mM phosphate buffer (pH = 7.0) using a peristaltic pump (flow rate ~ 150 $\mu L \cdot min^{-1}$). For force-extension analysis, we exclusively focus on torsionally unconstrained (nicked) tethers and calibrate the magnet distance-to-force relation for each bead by recording the transverse fluctuations of the beads at different magnet separations for times approximately 10-fold larger than the characteristic

time of the system at the corresponding force, and analyze the power spectral density of the fluctuations to quantify the force at each magnet position [9, 10]. The force (*F*) -extension (*z*) relation was subsequently fitted using an approximation of the worm-like chain model [11] to extract the contour length and bending persistence length of the DNA. Next, we record the force-extension behavior after flushing approximately 5 cell volumes of 10 mM PB buffer supplemented with 1-100 μM of either $Ru(TAP)_3^{2+}$ or $Ru(Phen)_3^{2+}$. In the presence of Ru-complex, we record magnet distance *vs.* tether extension (*z*) curves, and use the previously calibrated force for each bead to construct force *vs.* extension curves, which are fitted using the WLC model to give the contour length and persistence length as a function of complex concentration. For the construction of rotation curves, we focused on torsionally constrained DNA tethers and used the external magnets to introduce supercoiling at a tension *F* = 0.3 pN. Both clockwise and counterclockwise rotation of the magnets (with respect to the relaxed state) results in a symmetrical decrease of the extension due to plectonemic supercoil formation. We use the intersection of the extrapolated linear regimes of the rotation curves[12, 13] to define the midpoint of the rotation and to quantify the rotation offset as a function of added Ru(II)-complex with respect to midpoint of rotation curves obtained in the absence of added complex. Data analysis of magnetic tweezers data was performed using MATLAB (Mathworks). All quoted error bars are standard deviations obtained from multiple observations. Fitting uncertainties are 95% confidence intervals.

DNA-induced luminescence quenching. To study $Ru(TAP)_3^{2+}$ luminescence quenching by addition of DNA, we mixed either phage lambda DNA (NEB; dialyzed overnight against PB buffer) or a 32 bp double stranded fragment (obtained by annealing the complementary oligodeoxynucleotides 5' ACG TCA GTC AGC ATC AGA GTT TTC CCG TGA AG 3' and 5' CTT CAC GGG AAA ACT CTG ATG CTG ACT GAC GT 3') and $Ru(TAP)_3^{2+}$ at final concentrations c_{DNA} = 165 ng/mL and c_{Ru} = 5 μM. Emission spectra on excitation at 436 nm were recorded in the wavelength range 500-800 nm, employing a commercial spectrofluorometer (Fluoromax Plus; Horiba). The DNA concentration in the cuvette was stepwise decreased by replacing a fraction of the DNA solution with the same volume of a solution containing 5 μM $Ru(TAP)_3^{2+}$ in 10 mM phosphate buffer. The spectra were background corrected and further analyzed using MATLAB (Mathworks).

DNA photoreaction. To study photo-adduct formation of $Ru(TAP)_3^{2+}$ with DNA, we employed solutions containing 65 ng of DNA (either dialyzed phage lambda, or the annealed 32 bp oligo; see above) and 5 mM Ru(TAP)32+ in 10 mM phosphate buffer (pH = 7.0) in a final volume of 1 mL. The reactions were carried out in a quartz cuvette under irradiation of 465 nm light (Lumitronix) while being continuously stirred. After defined irradiation times, the absorbance of the solution was recorded in the range of 280 – 600 nm using an Evolution™ 201/220 UV-Vis-Spektrophotometer (ThermoFisher Scientific).

Supplementary Figures

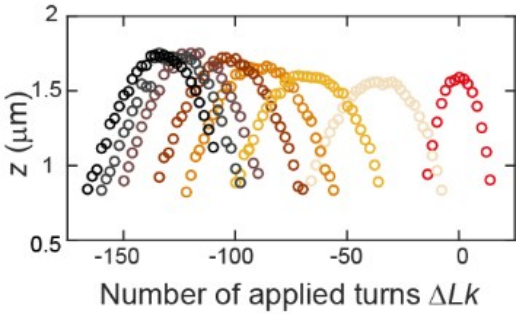

Figure S1. DNA unwinding by $Ru(Phen)_3^{2+}$. Rotation curves of DNA in the absence (red) and presence (brown gradient; see Figure 1 in the main text) of increasing concentrations (1-100 μM) of $Ru(TAP)_3^{2+}$.

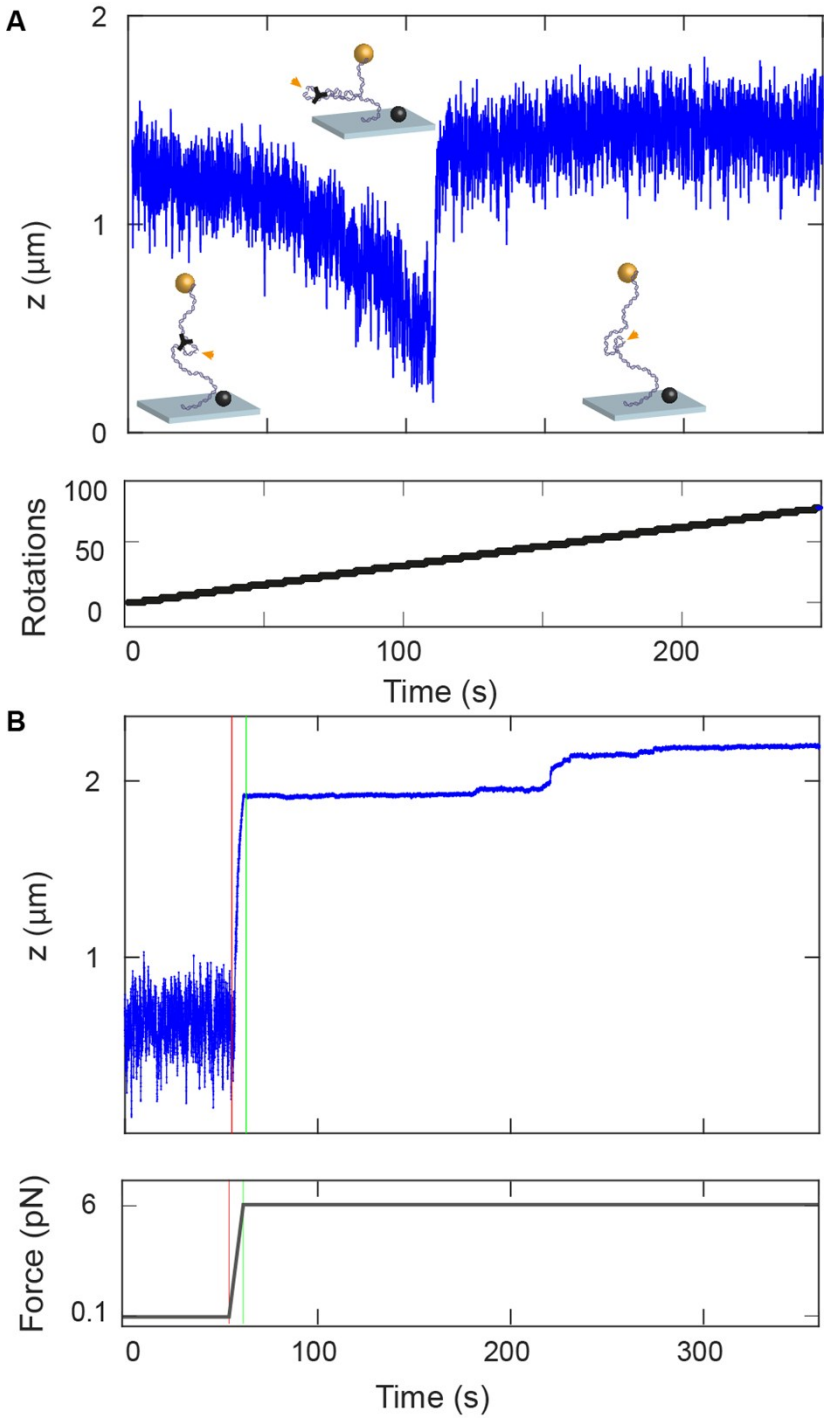

Figure S2. Evidence for $Ru(TAP)_3^{2+}$-mediated DNA looping. A. Rotation of a nicked DNA tether in the presence of 50 µM $Ru(TAP)_3^{2+}$ at F = 0.3 pN depicting extension decrease due to supercoiling, followed by a sudden extension jump to the relaxed state. Insets are schematic drawings (not to scale) demonstrating how multivalent binding by a single $Ru(TAP)_3^{2+}$ complex could shield the nick (orange arrow), thereby enabling introducing plectonemic supercoils that reduce the bead height. Dissociation (or partial dissociation) of the complex releases the topological constraint and removes the plectonemic supercoils by swivelling of the DNA at the nicking site, thereby restoring the extended state of the DNA. **B.** Force-jump experiment wherein DNA in the presence of 50 µM $Ru(TAP)_3^{2+}$ is first subjected to low tension (F = 0.1 pN) followed by a sudden increment in force (F = 6 pN). Note the discrete extension increments at high force.

Supplementary References

1. J. Lipfert, J. W. Kerssemakers, T. Jager and N. H. Dekker, *Nat Methods*, 2010, **7**, 977-980.
2. M. N. Ackermann and L. V. Interrante, *Inorganic Chemistry*, 1984, **23**, 3904-3911.
3. P. A. Wiggins, T. van der Heijden, F. Moreno-Herrero, A. Spakowitz, R. Phillips, J. Widom, C. Dekker and P. C. Nelson, *Nat Nanotechnol*, 2006, **1**, 137-141.
4. F. Kriegel, W. Vanderlinden, T. Nicolaus, A. Kardinal and J. Lipfert, *Methods Mol Biol*, 2018, **1814**, 75-98.
5. P. U. Walker, W. Vanderlinden and J. Lipfert, *Phys. Rev. E*, 2018, **98**, 042412.
6. J. Lipfert, X. Hao and N. H. Dekker, *Biophys J*, 2009, **96**, 5040-5049.
7. J. P. Cnossen, D. Dulin and N. H. Dekker, *Rev Sci Instrum*, 2014, **85**, 103712.
8. M. T. van Loenhout, J. W. Kerssemakers, I. De Vlaminck and C. Dekker, *Biophys J*, 2012, **102**, 2362-2371.
9. A. te Velthuis, J. W. J. Kerssemakers, J. Lipfert and N. H. Dekker, *Biophysical Journal*, 2010, **99**, 1292-1302.
10. B. M. Lansdorp and O. A. Saleh, *Rev Sci Instrum*, 2012, **83**, 025115.
11. C. Bouchiat, M. D. Wang, J. Allemand, T. Strick, S. M. Block and V. Croquette, *Biophysical Journal*, 1999, **76**, 409-413.
12. J. Lipfert, S. Klijnhout and N. H. Dekker, *Nucleic Acids Res*, 2010, **38**, 7122-7132.
13. F. Kriegel, C. Matek, T. Drsata, K. Kulenkampff, S. Tschirpke, M. Zacharias, F. Lankas and J. Lipfert, *Nucleic Acids Res*, 2018, **46**, 7998-8009.